LBL--18712

DE85 004608

LOOKING FOR ANOMALONS WITH A SEGMENTED CERENKOV DETECTOR

D.L. Olson

Lawrence Berkeley Laboratory
University of California
Berkeley, California 94720

October 1984

DISCLAIMER

This work was supported by the Director, Office of Energy Research, Division of Nuclear Physics of the Office of High Energy and Nuclear Physics of the U.S. Department of Energy under Contract Number DE-AC03-76SF00098.

Looking for Anomalons with a Segmented Cerenkov Detector

D. L. Olson
Nuclear Science Division, Lawrence Berkeley Laboratory
Berkeley, CA 94720

Introduction

I am reporting here on an experiment performed at the Lawrence Berkeley Laboratory Bevalac, Expt. 676H, to study the anomalon effect with a segmented total-internal-reflection Cerenkov detector. The participants in the experiment are listed in Table I. This experiment was largely a repeat of a previous experiment[1] with better detectors. In the previous experiment we used 3mm thick lucite radiators for our Cerenkov counters and had beams of ^{40}Ar at 1.88 GeV/nucleon and ^{56}Fe at 1.82 GeV/nucleon. For our latest run we had radiators of 3mm thick BK7W optical glass and 2mm thick fused silica and a beam of ^{40}Ca at 2.1 GeV/nucleon. The beam parameters for these different running periods are listed in Table II.

As a reminder, Fig. 1. shows the results we obtained with the lucite radiators and beams of iron and argon. One sees clearly that this previous experiment showed nothing anomalous.

The detector

A schematic view of a single element of the detector is shown in Fig. 2. The radiating material, optical quality BK7W glass or fused silica, is attached with a right angle elbow joint to a photomultiplier tube. The beam passes through perpendicular to the main face of the radiator and near the end opposite the PMT. These radiators have a slight taper, being wider at the PMT end. The effect of the taper, shown in the lower part of Fig. 2, is to put an upper limit on the optical path length to the PMT. Because of the geometry of these detectors, all faces being either parallel or perpendicular to the beam direction, the Cerenkov light emitted by particles with velocities above a certain threshold value, $\beta_T \approx 0.9$, is completely trapped by total-internal-reflection. The light will get out of the radiator only at the PMT which is optically coupled to it, or at

Table I. Bevalac Expt. 676H

participants	affiliation
M. Baumgartner	LBL
H. J. Crawford	UC SSL
J. P. Dufour*	CEN Bordeaux-Gradignan
J Girard**	CEA Saclay
D. E. Greiner	LBL
P. J. Lindstrom	LBL
D. L. Olson	LBL
T. J. M. Symons	LBL, spokesman

*Present address: Centre d'Etudes Nucleaires de Bordeaux-Gradignan, Le Haut Vigneau, F-33170 Gradignan, France.
**Present address: Commissariat a l'Energie Atomique de Saclay, F-91191 Gif-sur-Yvette Cedex, France.

Table II. Beam parameters

species	energy GeV/nucleon	no. primary interactions
^{40}Ar[a]	1.88	4.6×10^5
^{56}Fe[a]	1.62	9.1×10^5
^{40}Ca[b]	2.1	8.0×10^5

[a]Ref. 1.
[b]present results.

imperfections in the surface of the radiator.

If the direction of the incident particle is not perpendicular to the face of the radiator it is possible, for large enough incident angles, for the Cerenkov light to escape from and not be trapped in the radiator by total-internal-reflection. For the beam energies we used, the light is trapped for incident angles <3° and the response of the detector falls off very rapidly for larger angles. The net result of this effect is that these counters are sensitive only to particles with high velocities and small angles.

A diagram of the setup for this experiment is shown in Fig. 3. The beam is incident from the left and passes through a series of scintillation and Cerenkov counters. The primary trigger for this experiment was a 6X6 mm^2 scintillator. There were 6 mm thick lucite Cerenkov counters for charge in and charge out information in front of and behind the series of 43 thin counters. The 9 fused silica Cerenkov counters (2mm thick) and the 34 glass Cerenkov counters (3mm thick) provided both the target material and the charge measurements along the path of the beam.

The number of photons of Cerenkov light produced by a relativistic projectile fragment is proportional to $Z\beta$ so that the signal produced in a Cerenkov counter is proportional to $\sum_F Z\beta$, where the summation is over all of the projectile fragments produced in an interaction. The result of summing over Z^2 is that as long as the highest-charge fragment has a charge greater than about 1/2 the beam charge, these counters work quite well for measuring the charge of the most highly-charged fragment.

Figure 4 shows typical charge spectra for the counters we used. The upper plot is the charge spectrum produced by a single 2mm thick fused silica radiator with a resolution of $\sigma \approx 0.25e$; The lucite radiators of the earlier runs with Fe and Ar beams were similar to this. The lower plot is that for a single 3mm thick glass radiator showing the better charge resolution of $\sigma \approx 0.18e$. Figure 5 shows the charge spectra for secondary and tertiary fragments where the charge is determined by averaging over the path length for each fragment. Quite naturally, these spectra are sharper than those of Fig. 4 and one sees the broadening for lower charges that results from the Z^2 summation effect.

Figure 6 shows examples from the previous run with an ^{56}Fe beam of how the path length between interactions is determined. The plot shows the charge as determined by each counter in the series so that one is actually looking at the charge of the particle as it passes through the detector from left to right. The interaction points are located by noting the position at which a charge change is seen between adjacent counters. In general an interaction will occur somewhere inside a particular radiator. The signal from that counter will then be intermediate in value between that for the incoming and outgoing charges. By looking at the incoming and outgoing charges in two radiators to either side of the interaction one can locate the position of that interaction to a fraction of the thickness of the radiator. The resolution for doing this clearly depends upon the magnitude of the charge change in the interaction. The resolution we obtain with for $\Delta Z > 1$ interactions is significantly better than that for $\Delta Z = 1$ so that this report is only for $\Delta Z > 1$ reactions.

Analysis

The mean free paths, MFP's, determined in this experiment are computed with the following rather standard formulas.

$$\lambda_Z^*(x) = \frac{S_N(z,x)}{N(z,x)}$$

$$\frac{\Lambda^*(x)}{\Lambda^*_{>3cm}} = \frac{\lambda_Z^*(x)}{\langle \lambda_Z^* \rangle_{(x>3cm)\ Z}}$$

where $S_N(z,x)$ is the total path length up to the N'th interaction in the distance

interval at x for the charge z and $N(z,x)$ is the number of interactions for charge z in this interval. The mean free path averaged over charge $\Lambda^*(x)$ and normalized by the average value of this number for x>3cm is given by the second formula above where $\langle\lambda_Z^*\rangle_{(x>3cm)}$ is the average value of the MFP for charge z at distances greater than 3 cm and the ratio of λ_Z^*'s is then averaged over the different charges.

The λ_Z^* results are displayed in Fig. 7. The MFP of the primary beam, ^{40}Ca in this case, is shown in the upper left corner. One sees that it is quite constant with distance and it has the value of 8.01±0.04cm. The other MFP's shown in Fig. 7 are for the secondary charges indicated and it is apparent that there is no systematic dependence other than being constant with distance from the primary interaction point, x. The values of the $\langle\lambda_Z^*\rangle_{(x>3cm)}$ for these charges are listed in Table III.

The Λ^* values are commonly calculated by normalizing the λ_Z^* values by a power law dependence, $\lambda \propto Z^{-b}$, rather than to the measured individual MFP's as we have done. Figure 8 is provided as a comparison of these methods where the individual λ_Z^*'s are plotted vs. z and shown with the power law fit. In this case, we derived a value for b of 0.50 which lies within the range of 0.4 to 0.6 of the values that are often used. It should be noted however that the fit, χ^2=51 for 10 degrees of freedom, was not particularly good as is clearly seen in the figure.

The final result of our analysis is shown in Fig. 9. Just as one saw with the individual charge MFP's, one sees in the global summation that there is nothing anomalous in the reactions we investigated. The x bin width in this plot is 3mm and the first bin is the 6 to 9mm bin. The data in this figure are fit well by a horizontal line with χ^2=30 for 31 degrees of freedom. The curves drawn show what would be the effect of previously reported[2,3] admixtures of anomalons. It is obvious that neither of these curves is at all consistent with our data.

Summary

This experiment has confirmed our previous result, now with higher quality detectors and a different target material, that large projectile fragments of high energy heavy ions exhibit normal mean-free-paths for reactions with ΔZ>1 at distances greater than 6mm from the primary interaction point. The charge range for each beam we used is listed in Table IV. If anomalons exist they necessarily must have low velocity or low charge or be produced at large angles or result in $\Delta Z \leq 1$ reactions.

Table III. Mean Free Paths for x > 3cm.

charge	$\langle\lambda_Z^*\rangle_{(x>3cm)}$	χ^{2a}
20[b]	8.01±0.04	43
18	8.46±0.07	36
17	8.75±0.10	20
16	9.18±0.09	31
15	9.63±0.12	14
14	9.90±0.10	7
13	10.01±0.13	30
12	10.45±0.12	42
11	10.64±0.16	24
10	10.58±0.15	30

[a]for 23 degrees of freedom
[b]primary beam.

Table IV. Range of Covered Parameters

parameter	range
production angles	<3°
distance	> 6 mm
for secondary charges	13 - 24 from ^{56}Fe
	11 - 16 from ^{40}Ar
	10 - 18 from ^{40}Ca
reactions with	ΔZ>1

Acknowledgements

This work was supported by the Director, Office of Energy Research, Division of Nuclear Physics of the Office of High Energy and Nuclear Physics of the U.S. Department of Energy under Contract No. DE-AC03-76SF00098.

References

1 T. J. M. Symons, M. Baumgartner, J. P. Dufour, J. Girard, D. E. Greiner, P. J. Lindstrom, D. L. Olson, H. J. Crawford, Phys. Rev. Lett. *52*, 982 (1983).

2 E. M. Freidlander, R. W. Gimpel, H. H. Heckman, Y. J. Karant, Phys. Rev. C *27*, 1489 (1983).

3 M. L. Tincknell, P. B. Price, S. Perlmutter, Phys. Rev. Lett. *51*, 1948 (1983).

Figure 1

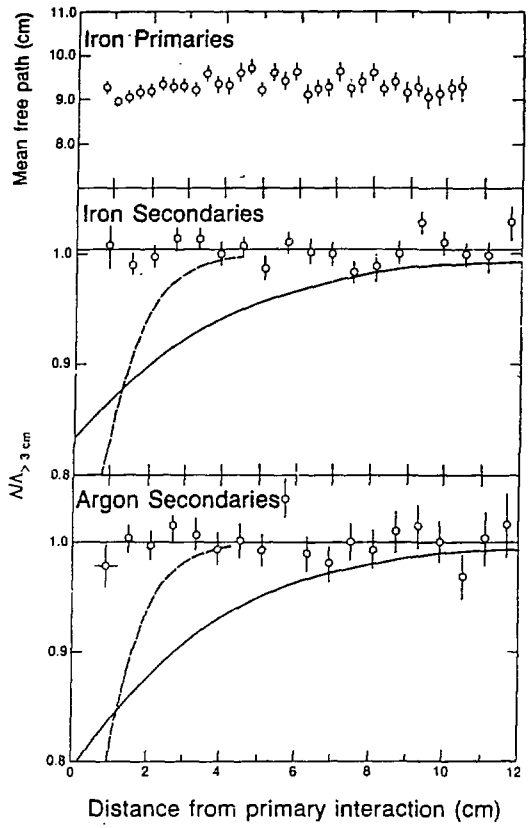

Previous results. See Ref. 1.

Figure 2

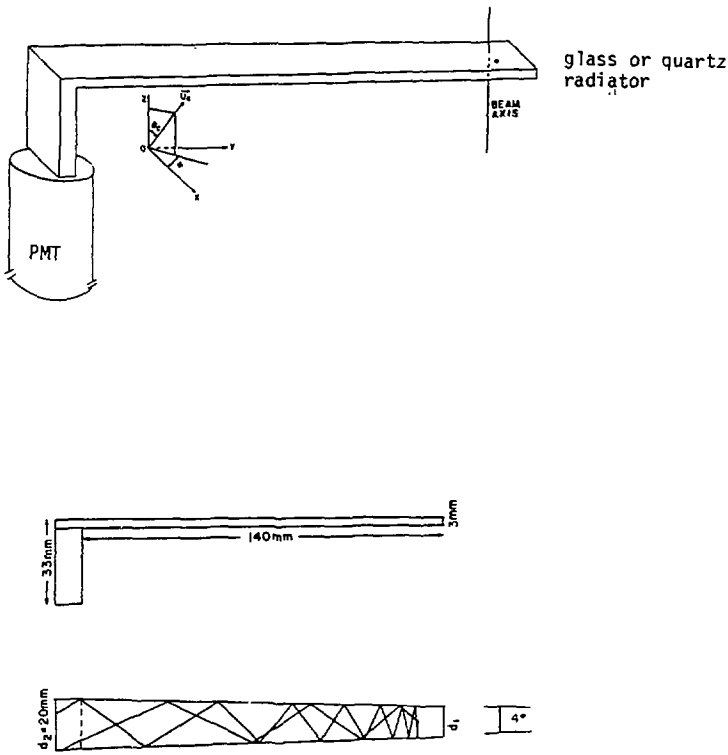

Single Cerenkov counter. Material is 2mm thick fused silica or 3mm thick BK7W glass. The beam passes through near the end opposite the PMT. The lines in the lower figure show the effect of the taper on the optical path.

Figure 3

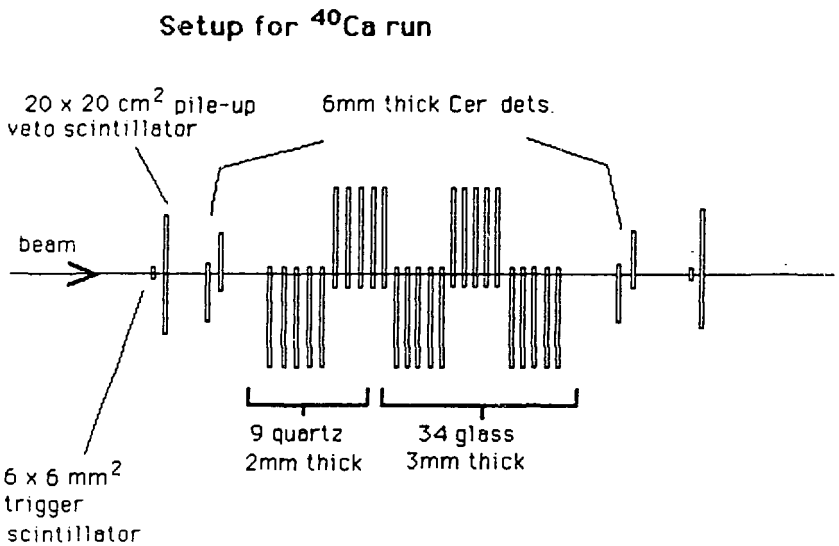

Schematic diagram of experimental setup.

Figure 4

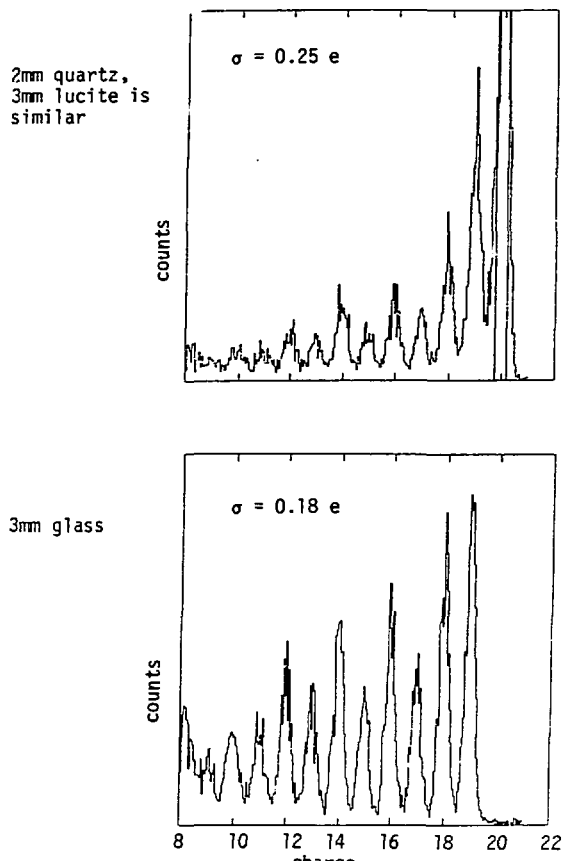

Typical charge spectra for a single 2mm thick fused silica radiator (upper) and a 3mm thick glass radiator (lower).

Figure 5

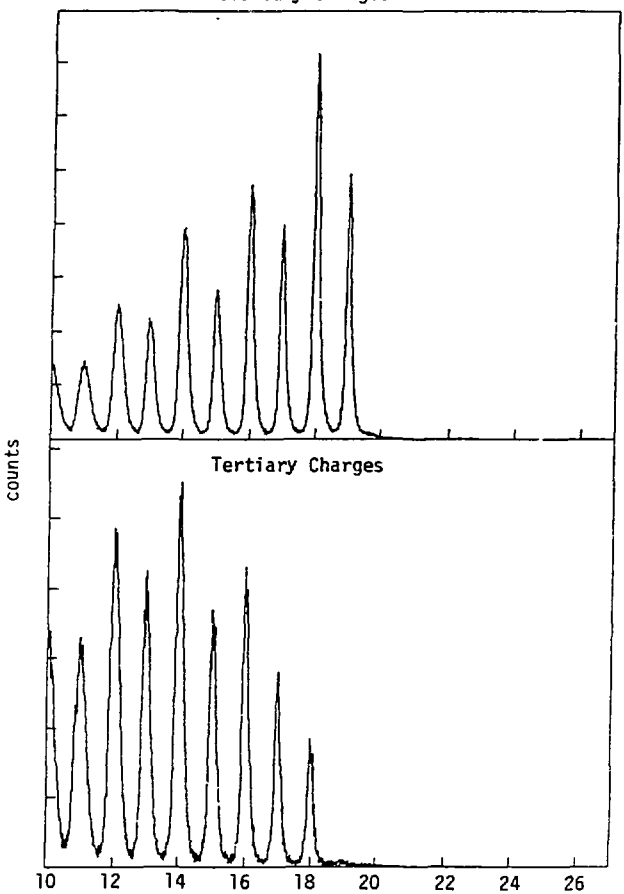

Charge spectra for secondary and tertiary fragments. The computed charge is averaged over the length of the secondary or tertiary path.

Figure 6

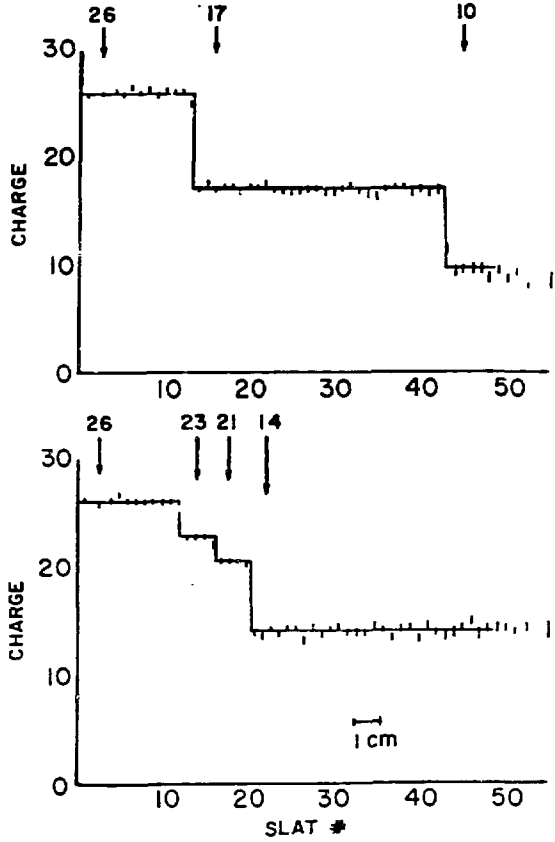

The measured charge in each Cerenkov counter vs. radiator position in the detector array. The beam passes through from left to right. These are two examples of individual events from the data of Ref. 1. The same procedure is used for the present data.

Figure 7

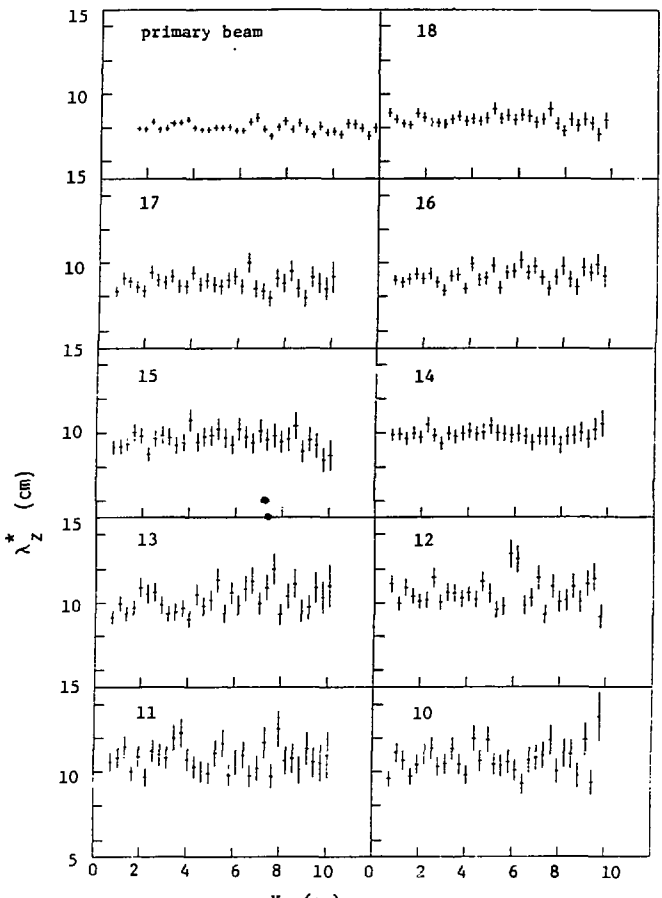

Mean free path vs. length of track. Horizontal scale is track length and vertical scale is the computed mean free path, both in cm. The upper left plot is for the primary beam of ^{40}Ca. The remaining plots are for secondary fragments with the charge indicated in each box. The vertical scale in each box ranges from 5 to 15 cm. The data points are for bins 3mm wide. The first bin for the primary beam is 15 to 18 mm. The first bin for the secondary fragments is 6 to 9 mm.

Figure 8

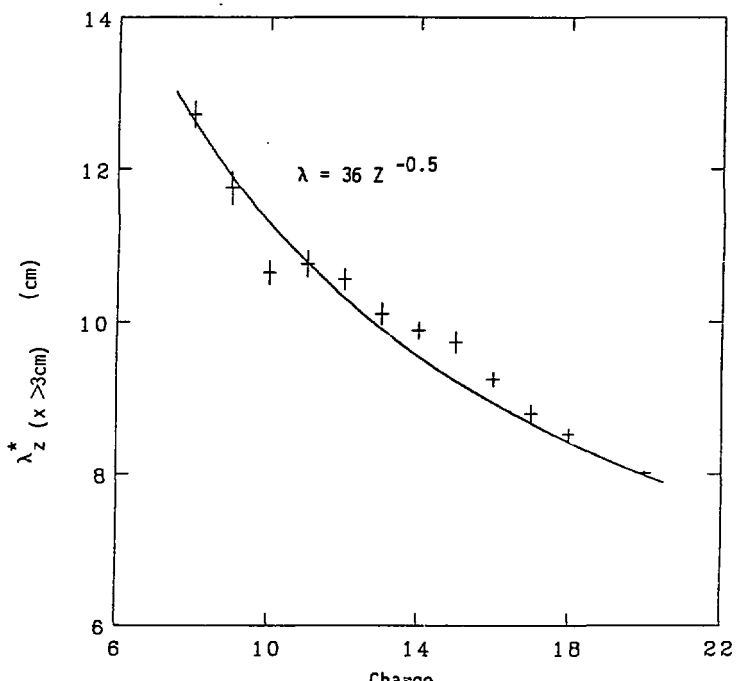

Average large-distance MFP for each charge. The curve is the result of fitting $10 \leq z \leq 20$ with a power law as indicated.

Figure 9

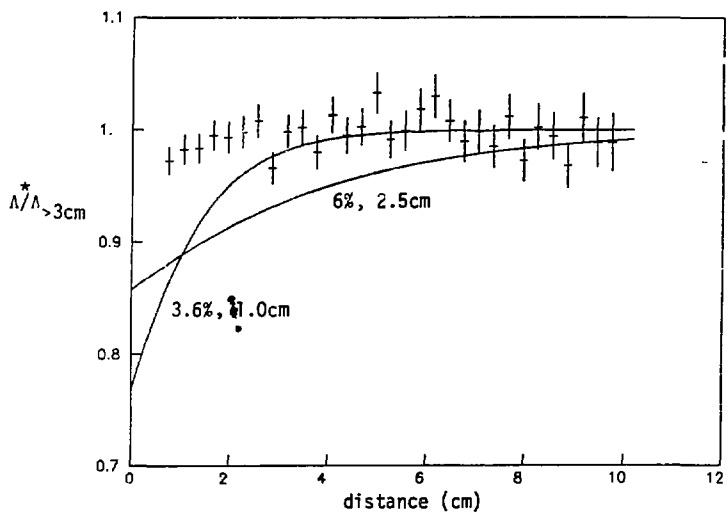

The charge-averaged secondary MFP vs. track length. The bins are 3mm wide and the first bin is for 6 to 9 mm. The curves show the effect of the anomalon results from Refs. 2 and 3.